



OpenMEEG: opensource software for quasistatic bioelectromagnetics

Alexandre Gramfort, Théodore Papadopoulo, Emmanuel Olivi, Maureen Clerc

► To cite this version:

Alexandre Gramfort, Théodore Papadopoulo, Emmanuel Olivi, Maureen Clerc. OpenMEEG: open-source software for quasistatic bioelectromagnetics. BioMedical Engineering OnLine, 2010, 9 (1), pp.45. 10.1186/1475-925X-9-45 . inria-00467061v2

HAL Id: inria-00467061

<https://inria.hal.science/inria-00467061v2>

Submitted on 27 May 2010

HAL is a multi-disciplinary open access archive for the deposit and dissemination of scientific research documents, whether they are published or not. The documents may come from teaching and research institutions in France or abroad, or from public or private research centers.

L'archive ouverte pluridisciplinaire **HAL**, est destinée au dépôt et à la diffusion de documents scientifiques de niveau recherche, publiés ou non, émanant des établissements d'enseignement et de recherche français ou étrangers, des laboratoires publics ou privés.

OpenMEEG: opensource software for quasistatic bioelectromagnetics

Alexandre Gramfort^{*1,2}, Théodore Papadopoulo¹, Emmanuel Olivi¹, Maureen Clerc^{1*}

¹Athena Project Team, INRIA Sophia Antipolis Méditerranée, France

²Parietal Project Team, INRIA Saclay Ile-de-France, France

Email: Alexandre Gramfort^{*} - alexandre.gramfort@inria.fr; Théodore Papadopoulo - theodore.papadopoulo@inria.fr; Emmanuel Olivi - emmanuel.olivi@inria.fr; Maureen Clerc^{*} - maureen.clerc@inria.fr;

^{*}Corresponding author

Abstract

Background: Interpreting and controlling bioelectromagnetic phenomena require realistic physiological models and accurate numerical solvers. A semi-realistic model often used in practise is the piecewise constant conductivity model, for which only the interfaces have to be meshed. This simplified model makes it possible to use Boundary Element Methods. Unfortunately, most Boundary Element solutions are confronted with accuracy issues when the conductivity ratio between neighboring tissues is high, as for instance the scalp/skull conductivity ratio in electro-encephalography. To overcome this difficulty, we proposed a new method called the symmetric BEM, which is implemented in the OpenMEEG software. The aim of this paper is to present OpenMEEG, both from the theoretical and the practical point of view, and to compare its performances with other competing software packages.

Methods: We have run a benchmark study in the field of electro- and magneto-encephalography, in order to compare the accuracy of OpenMEEG with other freely distributed forward solvers. We considered spherical models, for which analytical solutions exist, and we designed randomized meshes to assess the variability of the accuracy. Two measures were used to characterize the accuracy: the Relative Difference Measure and the Magnitude ratio. The comparisons were run, either with a constant number of mesh nodes, or a constant number of unknowns across methods. Computing times were also compared.

Results: We observed more pronounced differences in accuracy in electroencephalography than in magnetoencephalography. The methods could be classified in three categories: the linear collocation methods, that run very fast but with low accuracy, the linear collocation methods with isolated skull approach for which the accuracy is improved, and OpenMEEG that clearly outperforms the others. As far as speed is concerned, OpenMEEG is on par with the other methods for a constant number of unknowns, and is hence faster for a prescribed accuracy level.

Conclusions: This study clearly shows that OpenMEEG represents the state of the art for forward computations. Moreover, our software development strategies have made it handy to use and to integrate with other packages. The bioelectromagnetic research community should therefore be able to benefit from OpenMEEG with a limited development effort.

Introduction

Many devices used in the clinical or the cognitive science domain perform electromagnetic measurements, or stimulation, on the human body. Devices measuring electric fields include electro-encephalograms (EEG), -cardiograms (ECG), -myograms (EMG), while magneto-encephalograms (MEG) or magneto-cardiograms (MCG) measure magnetic fields. Among stimulating devices, transcranial magnetic stimulation (TMS) uses magnetic coils to stimulate brain regions, while functional electric stimulation (FES) and electrical impedance tomography (EIT) impose an electric current or potential through contact electrodes.

To interpret and control the bioelectromagnetic phenomena involved with these devices, realistic physiological modeling is required, in terms of geometry and conductivity [26]. Accurate numerical solutions of the governing equations must be computed: obtaining the best accuracy possible for a given computational model is one of the goals of OpenMEEG, the opensource software package introduced in this article.

Electromagnetic propagation is governed by the Maxwell equations, coupling the electrical and magnetic fields. This coupling simplifies when the relevant frequencies are low enough for the quasistatic regime to hold. The electric potential is then governed by the law of electrostatics

$$\nabla \cdot (\sigma \nabla V) = \nabla \cdot \mathbf{J}^P , \quad (1)$$

where σ is the conductivity field, and \mathbf{J}^P is a dipolar source distribution within the domain. When considering brain activations, it represents average postsynaptic currents within pyramidal cortical neurons. A boundary condition must be imposed, typically controlling the normal current on the domain boundary:

$$\sigma \nabla V \cdot \mathbf{n} = j . \quad (2)$$

The electric potential can be computed independently from the magnetic field, by solving (1) with boundary condition (2). The magnetic field \mathbf{B} depends both on the electric potential V and on the current source distribution \mathbf{J}^P , through the Biot and Savart law:

$$\mathbf{B}(\mathbf{r}) = \frac{\mu_0}{4\pi} \int (\mathbf{J}^P(\mathbf{r}') - \sigma \nabla V(\mathbf{r}')) \times \frac{\mathbf{r} - \mathbf{r}'}{\|\mathbf{r} - \mathbf{r}'\|^3} d\mathbf{r}' , \quad (3)$$

written here in the case where $j = 0$ on the boundary.

A *forward problem* consists of simulating V and/or \mathbf{B} when σ , \mathbf{J}^P , and boundary current j are known. The forward electro- magnetostatics problem is well-posed, in contrast to the far more difficult, ill-posed *inverse problem* of estimating σ , or \mathbf{J}^P , from partial boundary data. Still, obtaining an accurate solution for the

forward problem is far from trivial. This paper presents a software package, OpenMEEG, that makes available to the community recent research efforts to improve the accuracy of forward solvers.

Forward solutions provide the relationship between the quantities of interest and the measurements. To obtain a good description of this relationship, one must model the sources, the conductivity, and the sensors.

The choice of conductivity model is especially delicate because it strongly constrains the numerical solutions that can be used to solve the problem. In all generality, the conductivity field σ should be modeled as a tensor field, because composite tissues such as bone and fibrous tissues have an effective conductivity that is anisotropic. Realistic, anisotropic conductivity models can however be difficult to calibrate and handle; simpler, semi-realistic, conductivity models assign a different constant conductivity to each tissue, as depicted in Figure 1. There are three main types of conductivity models, and associated numerical methods:

1. if the conductivity field can be described using simple geometries (with axilinear, planar, cylindrical, spherical or ellipsoidal symmetry), *analytical methods* can be derived, and fast algorithms have been proposed that converge to the analytical solutions for EEG [8, 16] and MEG [25];
2. for piecewise constant conductivity fields as in Figure 1, *Boundary Element Methods* (BEMs) can be applied, resulting in a simplified description of the geometry only on the boundaries;
3. general non-homogeneous and anisotropic conductivity fields are handled by *volumic methods*; Finite Element Methods and Finite Difference Methods belong to this category.

This paper deals with Boundary Element Methods, whose advantage over volumic methods is to use an economic representation of the conductivity field (a few conductivity parameters - one per tissue, and a few triangular meshes to represent the interfaces). Until recently, all Boundary Element Methods used in bio-electromagnetics were based on a Green representation theorem, involving operators called single- and double-layer potentials. In OpenMEEG the approach is to consider an extended version of the Green representation theorem, involving more operators, and leading to a new BEM formulation, called the Symmetric Boundary Element Method.

The structure of the paper is as follows: the applications targeted by OpenMEEG are first presented, then some mathematical aspects of the Symmetric BEM are explained (details are presented in an appendix).

Then, to motivate the use of OpenMEEG, a comparison study with four other solvers in the context of

EEG forward modeling is presented. The accuracy of the solvers is tested on multiple random sphere models. The accuracy of OpenMEEG is also assessed by numerical experiments for MEG forward modeling. Finally a section provides technical details on the OpenMEEG software package while giving sample code for using OpenMEEG via Python or via the Fieldtrip Matlab toolbox. A second appendix presents a more complete presentation of the usage of OpenMEEG via a command line interface.

Target applications of OpenMEEG

The main purpose of OpenMEEG is to solve the forward problems arising in magneto- and electro-encephalography. A geometrical model of nested meshes representing tissue interfaces must be provided to OpenMEEG, which does not perform any segmentation or meshing. The main output of a forward problem is a leadfield, i.e., the linear application relating sources at specific locations to sensor measurements. Although the principal target of OpenMEEG is magneto- and electro-encephalography, other types of bioelectromagnetic problems have also been handled with OpenMEEG: we hereforth describe its current scope.

Electroencephalography (EEG) is concerned with the variations of electric potential on the scalp, due to sources within the brain. At frequencies of interest, the quasistatic regime is valid, resulting in the electrostatics relation (1). The air surrounding the scalp is supposed non-conductive, hence the normal current vanishes on the scalp: $j = 0$ in boundary condition (2). The sources within the brain are represented by dipoles: in equation (1), the sources are $\mathbf{J}^p = \vec{q}\delta_p$ where p is a dipole position and \vec{q} the associated dipolar moment. OpenMEEG computes the electric potential and the normal current on each interface between two homogeneous tissues, due to electric sources within the brain. EEG sensors are electrodes, modeled in OpenMEEG as discrete positions on the scalp at which the potential can be measured (infinite impedance assumption). On these sensors, OpenMEEG computes the EEG leadfield, representing the linear relationship between source amplitude (for fixed position and orientation) and sensor values.

Magnetoencephalography (MEG) is concerned with magnetic fields produced by sources within the brain, which, like for EEG, are modeled as dipoles [13]. OpenMEEG makes use of the Biot and Savart relation (3) to compute the magnetic field, and hence requires the electric potential to be computed beforehand on all the interfaces [9]. Magnetometers or gradiometers can be modeled in OpenMEEG. Magnetometers are defined by their position and the direction of the field they measure. Gradiometers and

more general sensors are handled by providing to OpenMEEG the positions, the orientations and the weights of integration points. For example with axial gradiometers present in CTF MEG systems, the forward field for a sensor is obtained by subtracting the two leadfields computed at the locations of two nearby magnetometers.

Electrical Impedance Tomography (EIT) infers characteristics of a conductive domain, by analyzing the potential resulting from the application of a current on the boundary. This method has been applied to calibrate the conductivity of EEG head models [3,4,11]. OpenMEEG computes the forward problem associated to EIT: given a conductive domain Ω defined by the interfaces between homogeneous regions, and their conductivity, and for a prescribed normal current j , OpenMEEG computes the potential V and the normal current $\sigma \partial_{\mathbf{n}} V$ on each interface by solving (1) for $\mathbf{J}^P = 0$, and with boundary condition (2). Similarly to EEG, the potential is interpolated onto the electrode positions.

Intracranial electric potentials are measured in certain clinical settings, either on the surface (ElectroCorticography) or within the brain (intracranial EEG, or stereotaxic EEG). OpenMEEG is able to compute leadfields for such intracranial electrodes, in realistic head models.

Functional Electrical Stimulation (FES) provides a way to restore movement of paralyzed body regions by activating the efferent somatic axons. For this a current is applied to a nerve sheath, using specially designed electrodes. The precise location and time course of the applied current must be optimized in order to achieve the best selectivity, and to minimize the current intensity for a desired outcome. Optimizing the stimulation parameter in a realistic nerve model requires a forward model for FES. OpenMEEG provides such a tool, by combination of the concepts of EIT and of internal potential simulation (see section on the applications targeted by OpenMEEG) [15,19].

Cortical Mapping is an *inverse problem* that aims to recover the potential and the normal current occurring on the surface of the cortex (i.e., under the skull bone), given EEG measurements on electrodes [14]. A particularly elegant solution to this problem has been proposed with the symmetric BEM [6], making it possible e.g. to solve further source localization problems.

Methods: implementation

OpenMEEG uses a Galerkin Boundary Element formulation, that jointly considers the electric potential and the normal current on each interface as unknowns of the problem. A P1 (piecewise linear) approximation is used for the electric potential, whereas the normal current $\sigma \frac{\partial V}{\partial \mathbf{n}}$ is approximated with P0

(piecewise constant) boundary elements. The most intricate part of the implementation concerns the assembly of the system matrix, requiring singular kernel integration over triangles. Those are double integrals. The inner integrals are computed with analytical schemes [7], whereas the outer integrals are computed with a 7-point Gauss quadrature scheme [2]. An adaptive integration scheme recursively subdivides the triangles until the required precision is achieved. This adaptive integration has an influence on the accuracy, as will be exposed in the benchmark results further on.

Since the electric potential can only be computed up to a constant, the system matrix is deflated to make it invertible. In practice, it consists of imposing the constraint that the integral of the potential over the external layer is 0.

The magnetic field is computed by using the Biot and Savart equation with the Galerkin piecewise linear approximation for the potential [9].

As stated above, given a set of dipole positions and orientations, a set of sensors and a head model defining homogeneous conductivity regions, the M/EEG forward problem produces as output the *leadfield*.

OpenMEEG computes such leadfields with the following procedure (see figure 13 on page 36 for a detailed graphical representation of this flowchart):

- assemble the system matrix involving boundary integral operators on the discretized surfaces;
- for a specified set of dipole positions and orientations, assemble a discretized, source-related term;
- solve the linear system relating the two above matrices (providing V and $\sigma \frac{\partial V}{\partial \mathbf{n}}$ on each interface)
- interpolate the scalp potential (for EEG) or apply the discretized Biot and Savart relation (for MEG).

Mathematical details, as well as the practical usage of OpenMEEG can be found in the Appendix.

Methods: benchmark comparison study

In order to motivate the use of the OpenMEEG software, we have conducted a set of numerical experiments that compare the accuracy and the robustness of OpenMEEG with alternative M/EEG forward solvers. The comparison in the context of EEG forward modeling is run with the 4 alternative BEM solvers. The precision of the MEG forward solver is demonstrated using known analytical properties of the magnetic field when considering sphere models and with two other solvers.

Publicly available M/EEG forward solvers Several software projects have the ability to solve the M/EEG forward problems: MNE, BrainStorm, EEGLAB (via the NFT Toolbox), Fieldtrip, Simbio, OpenMEEG and SPM, which shares with Fieldtrip the same M/EEG forward solvers.

Fieldtrip and SPM offer two implementations of the BEM. The first one, called *Dipoli*, was written by Oostendorp [23] and is not open source (only binary files for UNIX systems are available), while the second one, called *BEMCP*, is opensource and was written by Christophe Phillips during his PhD [24]. The *Dipoli* solver implements a linear collocation method with Isolated Skull Approach (ISA) [12], whereas *BEMCP* implements a simple linear collocation method. The *Dipoli* implementation details can be found in [23]. Another implementation with linear collocation (with and without ISA) can be found in the Matlab toolbox called Helsinki BEM [27]. The MNE package written in pure C code by Hämäläinen also offers a linear collocation (with ISA) implementation of the BEM. The Brainstorm toolbox in its latest version uses only sphere models for both EEG and MEG. Recently the EEGLAB toolbox also has provided a package called NFT that is based on a BEM called METU [1]. Finally, the Simbio forward solver also consists of a BEM with linear collocation and ISA.

Commercial software packages are not listed here. However, to our knowledge, commercial products that provide a BEM solver for forward modeling implement a linear collocation method with ISA. This is for example the case of ASA [29].

Accuracy measures The accuracy of forward solvers can be assessed for simple geometries such as nested spheres, by comparison with analytical results. The precision of a forward solution is tested with two measures: the RDM (Relative Difference Measure) and the MAG (Magnitude ratio) [20].

The RDM between the forward field given by a numerical solver g_n and the analytical solution g_a is defined as:

$$RDM(g_n, g_a) = \left\| \frac{g_n}{\|g_n\|} - \frac{g_a}{\|g_a\|} \right\| \in [0, 2] ,$$

while the MAG between the two forward fields is defined as:

$$MAG(g_n, g_a) = \frac{\|g_n\|}{\|g_a\|} .$$

In both of these expression, the norm is the discrete ℓ^2 norm over the set of sensor measurements. The closer to 0 (resp. to 1) the RDM (resp. the MAG), the better it is.

Geometrical models The comparisons were made both on classic regular sphere meshes as in figure 2 on page 27, and on random meshes. A random sphere mesh with unit radius and N vertices is obtained by randomly sampling 10N 3D points, normalizing them, meshing their convex hull and decimating the

obtained triangular mesh from $10N$ to N vertices. This process guarantees an irregular meshing while avoiding flat triangles. The BEM solvers are tested with three nested sphere shells which model the inner and outer skull, and the skin. The radii of the 3 layers are set to 88, 92 and 100, while the conductivities of the 3 homogeneous volumes are set to 1, $1/80$ (skull) and 1^1 . For each randomly generated head model, it was tested that they were no intersection between each mesh. For every head model, solvers are tested with the same 5 dipoles positioned on the z-axis with orientation (1,0,1) and various distances to the inner layer (cf. figure 2 on page 27). As expected, the accuracy of the solvers decreases as this distance gets small.

Results

Results: accuracy of the electric potential simulations The implementations tested for EEG are: OpenMEEG with and without adaptive numerical integration (abbr. OM and OMNA), Simbio (abbr. SB), Helsinki BEM with and without ISA (abbr. HBI and HB), Dipoli (abbr. DP) and BEMCP (abbr. CP). The METU solver was also tested but we were unable to obtain the precisions advertised in [1], so it was decided not to include it in the comparison.

The results with regular sphere meshes are presented in figure 3 on page 28 for 3 different point samplings on each interface. The coarsest sampling has only 42 vertices per interface and 42 EEG electrodes, the intermediate one has 162 points per interface and 162 EEG electrodes, and the finest sampling has 642 points per interface and 642 EEG electrodes. In this case, electrodes are simply located at mesh nodes. From these simulations it can be observed that:

- HB and CP, that implement a simple linear collocation method, have similar results and are clearly the less precise solvers.
- HBI, SB and DP, that implement a linear collocation method with ISA, have very similar results. SB and HBI are however slightly more accurate than DP.
- OpenMEEG provides the most precise solutions even when no adaptive integration is used. The adaptive integration significantly improves the results, particularly when the meshes are coarsely sampled (42 and 162 vertices per layer).

Simulations have also been run on a large number of randomly sampled sphere meshes, in order to compare the robustness of the different solvers. Each result is obtained by running all solvers on 100 random head

¹In this benchmark, the units are arbitrary, but in practise, units should be expressed with the International System of Units (SI).

models. The mean accuracy measures (RDM and MAG) are represented using boxplots, in order to display the variance of the errors. Figure 4 presents the boxplots obtained by running the solvers on random head models with either 600 or 800 vertices per interface. These results lead to the same ranking of methods as those of Figure 3, if the average accuracy is considered. However the variances are also very informative, as they tell us about the precision. It can be observed that OM is not only very accurate, but also very precise because of its very small variance, which is an appreciable feature. The OMNA solver is also accurate but less precise: it has a larger variance. This demonstrates that the adaptive integration makes the solver more robust to irregular meshing. SB and HBI give, as expected, very similar results. One can also observe that the variances observed for CP and HB are significantly larger than for the other solvers, meaning that the collocation based BEM without ISA is very sensitive to irregular meshing.

As explained in the previous section, OpenMEEG considers as unknowns both the potential at vertices, and the normal current at the centers of the triangles. For a fair comparison with respect to numerical complexity, the previous experiments have been repeated with the constraint that each solver should handle *an equal number of unknowns*. This leads to considering meshes for OpenMEEG with less points than for others solvers. A closed triangular mesh with n vertices contains $2n - 4$ triangles and the normal current is not discretized for the outer layer as it is fixed to be 0. For a three-layer BEM, OpenMEEG therefore has to handle $7n - 8$ unknowns, while for a standard BEM this number is simply $3n$. For a fixed number n_u of unknowns, the number of vertices per layer n_{om} for OpenMEEG is $n_{om} = (n_u + 8)/7$ while for a standard BEM the number of vertices n_{std} is $n_{std} = n_u/3$. Results with 1500 and 3000 unknowns are presented in figure 4. It can be observed that OpenMEEG with adaptive integration still outperforms other solvers in term of mean accuracy as well as variance of the results. It is followed by DP, HBI and SB, that give also quite accurate solutions. OpenMEEG without adaptive integration is in this simulation behind DP, HBI and SB but remains more precise than HB and CP.

Results: accuracy of the magnetic field simulations We next present results for MEG forward modeling. MEG manufacturers propose 3 kinds of sensors (magnetometers, axial gradiometers, and planar gradiometers), all of which are oriented radially with respect to the helmet.

With a nested sphere model, Ohmic volume currents do not contribute to the radial component of the magnetic field [25] (the term containing $\sigma \nabla V$ in (3) vanishes). The MEG community commonly uses analytical solutions on spheres to compute MEG leadfields although volume currents do have an influence on the magnetic field when considering realistic head models [28]. OpenMEEG (as well as Simbio) uses the

previously computed electric potential on all surfaces to compute the contribution of the volume currents to the magnetic field at sensors. These considerations lead to two different setups to validate the MEG forward solutions provided by OpenMEEG. To do so, experiments have been run with two types of sensors: a set of magnetometers all oriented in the Cartesian direction $(1, 0, 1)$ and located at a distance of 120 from the center of the spheres, and a set of magnetometers at the same locations but radially oriented. In these experiments, we compared the analytical results with the solutions given by Simbio, by OpenMEEG with and without adaptive integration (abbr. OM and OMNA). We used a 3-layer model, and also a single layer model (the inner skull) as commonly done in practice. The single layer solution is abbreviated OM1L. The Fieldtrip Toolbox provides a solution to the MEG forward problem on realistic volume conductors which is not based on the Biot and Savart law but Helmholtz’s reciprocity principle [22]. This solver proposed by Nolte is abbreviated NT in the comparison results. Figure 6 presents the results with non-radial magnetometers, while figure 7 on page 32 presents the results obtained with radial magnetometers. From figure 6 on page 31 it can be observed that OpenMEEG provides solutions that are considerably more precise with the adaptive integration method. The results of Simbio and OpenMEEG with adaptative integration are mesh-dependent, whereas Nolte’s solver outperforms OpenMEEG and Simbio. In figure 7 on page 32, one can notice the correct cancellation of the volume current when the mesh size increases (notice the change of scale on the vertical axis). The OpenMEEG and Simbio solvers take the lead for radially oriented sensors with similar results for both.

Results: computation speed We have compared the computation times of EEG forward solvers in two situations: with a fixed number of vertices per layer, and with a fixed number of unknowns. When the number of vertices is fixed, the higher number of unknowns in the symmetric BEM makes the problem size larger. This is confirmed by the results presented in figure 8(a) on page 33 where it can be observed that OpenMEEG is slower than all solvers except Simbio. One explanation is that Simbio does not use BLAS/LAPACK for efficient linear algebra but implements its own routines in C code. When the number of unknowns is fixed (cf. figure 8(b) on page 33), the computation time of OpenMEEG is comparable with Dipoli and even slightly lower for highly sampled models. In all cases the collocation methods without ISA (HB and CP) are significantly faster, but their limited accuracy does not make them good candidates for EEG forward modeling. By jointly analyzing Figures 5 and 8(b), one can note that OpenMEEG is the fastest method for a prescribed accuracy.

The OpenMEEG Software Package

All the tests performed in this paper were made using the version 2.0 of OpenMEEG.

Licence OpenMEEG is distributed under the French opensource license CeCILL-B. It is intended to give users the freedom to modify and redistribute the software. It is therefore compatible with popular opensource licenses such as the GPL and BSD licenses. The CeCILL-B license imposes to anybody distributing a software incorporating OpenMEEG the obligation to give credits (by citing the appropriate publications), in order for all contributions to be properly identified and acknowledged².

Source code OpenMEEG is implemented in C/C++ with limited external dependencies. It uses the Intel MKL libraries on Windows and ATLAS (BLAS/LAPACK) on Unix systems for fast and accurate linear algebra. A modified version of the MATIO library³ has been integrated in OpenMEEG for Matlab compatible IOs for vectors and matrices. The source code of OpenMEEG is hosted on the INRIA GForge platform and is accessible to an anonymous user via the Subversion⁴ version control system. OpenMEEG binaries and source code are both available from <http://openmeeg.gforge.inria.fr>.

Multiplatform OpenMEEG is available as precompiled binaries for GNU-Linux systems, Mac OS and Windows. OpenMEEG's build and packaging system is based on *CMake/CPack*⁵ allowing easy development and deployment on all architectures.

Parallel processing Compilation of OpenMEEG can be done using advanced features provided by modern compilers. OpenMP is a technology that enables parallel computation at a limited cost in terms of software design. When OpenMEEG is compiled using OpenMP, the numerical integration, on which most of the computation time is spent, can be run in parallel. On a machine with 8 CPUs a standard EEG leadfield is computed up to 6 times faster.

Testing Deployment on multiple architectures with heterogenous hardware and software environments requires testing procedures to assess the stability of the solutions provided by compiled binaries. This testing procedure is run through the *CMake/CTest* testing software. OpenMEEG test suite guarantees the integrity of the results obtained by MEG, EEG and EIT forward solvers. A part of the tests consists of running OpenMEEG on a 3-layer spherical geometry like the one presented in figure 2. Outputs are then compared to analytical results to test that the accuracy is not degraded by a modification of the code.

²References to be acknowledged: [17], and the present article.

³<http://sourceforge.net/projects/matio>

⁴<http://subversion.tigris.org>

⁵<http://www.cmake.org>

Integration Considerable efforts have been made to facilitate the use of OpenMEEG by the M/EEG community. OpenMEEG can be simply invoked via a command line interface, or via higher levels languages. OpenMEEG can also be called from Python or via the Fieldtrip Toolbox, where it has been fully integrated in the M/EEG forward modeling routines.

For sample scripts using Python and Fieldtrip, see table 1 on page 37 and table 2 on page 38.

Benchmark The benchmark presented in the previous section was run within the Fieldtrip environment and its MATLAB source code can be obtained for noncommercial use from the authors. Since SPM uses the same code as Fieldtrip for forward modeling, SPM can now benefit from integration of OpenMEEG. Moreover, the binary format used by OpenMEEG is that of Matlab, by use of the opensource MATIO library.

A sample dataset for M/EEG forward modeling can be downloaded from <http://openmeeg.gforge.inria.fr>. The sample dataset is provided with scripts that can be run to compute MEG and EEG leadfields on a realistic 3-layer model.

Documentation A tutorial for OpenMEEG is available on the web site, and it is briefly summarised in the appendix at the end of this article. The tutorial describes the low-level interface and details the different steps to be followed when computing M/EEG leadfields. Developer documentation can be generated via doxygen⁶.

Conclusion

In this paper, the OpenMEEG software project has been detailed, from the mathematical grounds of the symmetric BEM to more practical aspects.

The relevance of the OpenMEEG solver for quasistatic bioelectromagnetics has been demonstrated by a benchmark incorporating many alternative solvers in the context of M/EEG forward modeling. According to the results of this simulation study, OpenMEEG outperforms all the alternative solvers tested. By providing state-of-the-art solutions for both EEG and MEG forward problems, OpenMEEG enables the combined use of these two complementary modalities.

It should be mentioned that OpenMEEG is being used for many problems in the field of quasistatic bioelectromagnetics, including Electrical Impedance Tomography, Intracranial electric potentials, Functional Electrical Stimulation and Cortical Mapping. This wide range of application domains, as well as its integration into high-level languages make OpenMEEG unique and particularly valuable for basic

⁶<http://www.stack.nl/~dimitri/doxygen/>

and clinical research purposes.

Authors' contributions

MC with TP and some other colleagues are at the origin of the mathematical developments of the symmetric BEM. AG designed most of the comparison framework detailed in this paper and carried it out. EO carried out the comparison for MEG. All the authors are the current main developpers of the OpenMEEG software package, with AG and TP playing the role of maintainers. AG led the integration effort with other toolboxes. All coauthors participated in writing the paper.

Acknowledgements

The authors acknowledge support from the ANR grant ViMAGINE ANR-08-BLAN-0250-02, and for EO from a PhD grant from the Regional Council of Provence Alpes Cote d'Azur. Help is gratefully acknowledged from C. Micheli and R. Oostenveld regarding the integration of OpenMEEG within Fieldtrip, and from A. Anwander, M. Dannhauer and C. Wolters regarding the use of Simbio.

Competing interests

The authors declare that they have no competing interests.

References

1. Zeynep Akalin-Acar and Nevzat G Gençer. An advanced boundary element method (bem) implementation for the forward problem of electromagnetic source imaging. *Physics in medicine and biology*, 49(21):5011–28, 2004.
2. Marc Bonnet. *Boundary Integral Equations Methods for Solids and Fluids*. John Wiley and Sons, 1999.
3. M. Clerc, G. Adde, J. Kybic, T. Papadopoulos, and J.-M. Badier. In vivo conductivity estimation with symmetric boundary elements. In Jaakko Malmivuo, editor, *International Journal of Bioelectromagnetism*, volume 7, pages 307–310, 2005.
4. M. Clerc, J.-M. Badier, G. Adde, J. Kybic, and T. Papadopoulos. Boundary element formulation for electrical impedance tomography. In *ESAIM: Proceedings*, volume 14, pages 63–71. EDP Sciences, sep 2005.
5. M. Clerc, A. Dervieux, O. Faugeras, R. Keriven, J. Kybic, and T. Papadopoulos. Comparison of bem and fem methods for the e/meg problem. In *Proceedings of BIOMAG Conference*, aug 2002.
6. M. Clerc and J. Kybic. Cortical mapping by Laplace-Cauchy transmission using a boundary element method. *Inverse Problems*, 23:2589–2601, 2007.
7. J. C. de Munck. A linear discretization of the volume conductor boundary integral equation using analytically integrated elements. *IEEE Trans. Biomed. Eng.*, 39(9):986–990, September 1992.
8. J.C. de Munck and M.J. Peters. A fast method to compute the potential in the multisphere model. *IEEE Trans. on Biomed. Engin.*, 40(11):1163–1174, 1993.
9. A. S. Ferguson, X. Zhang, and G. Stroink. A complete linear discretization for calculating the magnetic field using the boundary element method. *IEEE Trans. Biomed. Eng.*, 41(5):455–459, May 1994.

10. D. B. Geselowitz. On bioelectric potentials in an homogeneous volume conductor. *Biophysics Journal*, 7:1–11, 1967.
11. S. Gonçalves, J.C. de Munck, J.P. Verbunt, R.M. Heethaar, and F.H. Lopes da Silva. In vivo measurement of the brain and skull resistivities using an EIT-based method and the combined analysis of SEF/SEP data. *IEEE Transactions on Biomedical Engineering*, 50(9):1124–8, September 2003.
12. M. S. Hämäläinen and J. Sarvas. Realistic conductivity geometry model of the human head for interpretation of neuromagnetic data. *IEEE Trans. Biomed. Eng.*, 36(2):165–171, February 1989.
13. Matti Hämäläinen, Riitta Hari, Risto J. Ilmoniemi, Jukka Knuutila, and Olli V. Lounasmaa. Magnetoencephalography— theory, instrumentation, and applications to noninvasive studies of the working human brain. *Reviews of Modern Physics*, 65(2):413–497, April 1993.
14. Bin He, Yunhua Wang, and Dongsheng Wu. Estimating cortical potentials from scalp EEGs in a realistically shaped inhomogeneous head model by means of the boundary element method. *IEEE Transactions on Biomedical Engineering*, 46(10):1264–1268, October 1999.
15. S. Jacquir, J. Fruitet, D. Guiraud, and M. Clerc. Computation of the electrical potential inside the nerve induced by an electrical stimulus. In *EMBC 2007: Proceedings of the 29th Annual International Conference of the IEEE Engineering in Medicine and Biology Society*, 2007.
16. F. Kariotou. Electroencephalography in ellipsoidal geometry. *J. Math. Anal. Appl.*, (290):324–42, 2004.
17. J. Kybic, M. Clerc, T. Abboud, O. Faugeras, R. Keriven, and T. Papadopoulos. A common formalism for the integral formulations of the forward EEG problem. *IEEE Transactions on Medical Imaging*, 24:12–28, jan 2005.
18. J. Kybic, M. Clerc, O. Faugeras, R. Keriven, and T. Papadopoulos. Generalized head models for MEG/EEG: boundary element method beyond nested volumes. *Physics in Medicine and Biology*, 51:1333–1346, 2006.
19. J. Laforêt, D. Guiraud, and M. Clerc. A toolchain to simulate and investigate selective stimulation strategies for fes. In *EMBC 2009: Proceedings of the 30th Annual International Conference of the IEEE Engineering in Medicine and Biology Society*, 2009.
20. J. W. H. Meijs, O. W. Weier, M. J. Peters, and A. van Oosterom. On the numerical accuracy of the boundary element method. *IEEE Trans. Biomed. Eng.*, 36:1038–1049, 1989.
21. Jean-Claude Nédélec. *Acoustic and Electromagnetic Equations*. Springer Verlag, 2001.
22. G. Nolte. The magnetic lead field theorem in the quasi-static approximation and its use for magnetoencephalography forward calculation in realistic volume conductors. *Physics in Medicine and Biology*, 48:3637–3652, oct 2003.
23. T.F. Oostendorp and A. van Oosterom. Source parameter estimation in inhomogeneous volume conductors of arbitrary shape. *IEEE Trans. Bioned. Engin.*, 36:382–391, 1989.
24. C. Phillips. *Source estimation in EEG*. PhD thesis, Université de Liège, 2000.
25. Jukka Sarvas. Basic mathematical and electromagnetic concepts of the biomagnetic inverse problem. *Phys. Med. Biol.*, 32(1):11–22, 1987.
26. M. Soleimani, R.J. Shipley, N. Smith, and C.N. Mitchell. Medical imaging and physiological modelling: linking physics and biology. *BioMedical Engineering OnLine*, 8(1), 2009.
27. M. Stenroos, V. Mäntynen, and J. Nenonen. A matlab library for solving quasi-static volume conduction problems using the boundary element method. *Comput. Methods Prog. Biomed.*, 88(3):256–263, 2007.
28. R. Van Uiter, C. Johnson, and L. Zhukov. Influence of head tissue conductivity in forward and inverse magnetoencephalographic simulations using realistic head models. *IEEE Trans. on Biomed. Engin.*, 51(12):2129–2137, 2004.
29. F. Zanow and T.R. Knosche. Asa-advanced source analysis of continuous and event-related eeg/meg signals. *Brain Topography*, 16:287–290(4), 2004.

Appendix

The symmetric BEM

In early numerical experiments to compare a Boundary Element and a Finite Element Method (FEM) for forward electroencephalography, we found a superior accuracy of the FEM [5]. This triggered a quest to improve the precision of Boundary Element Methods and led us to study the extended Green representation theorem [21]. We proposed a common formalism for the integral formulations of the forward EEG problem, and derived three different Boundary Element Methods within the same framework [17]. In this section we recall the mathematical background of Boundary Element Methods, and present both the double-layer BEM, which is the most widespread method, and the symmetric BEM, which is a new formulation.

Green Representation

A fundamental result in potential theory shows that a harmonic function (i.e., such that $\Delta u = 0$) is uniquely determined within a domain Ω from its value on the boundary $\partial\Omega$ (Dirichlet condition), or the value of its normal derivative (Neumann condition). The Green Representation Theorem gives an explicit representation of a piecewise-harmonic function as a combination of boundary integrals of its jumps and the jumps of its normal derivative across interfaces. Before stating this theorem, some notation must be defined:

- The restriction of a function f to a surface S_j is indicated by f_{S_j} .
- The functions $f_{S_j}^-$ and $f_{S_j}^+$ represent the interior and exterior limits of f on S_j :

$$\text{for } \mathbf{r} \in S_j, \quad f_{S_j}^\pm(\mathbf{r}) = \lim_{\alpha \rightarrow 0^\pm} f(\mathbf{r} + \alpha \mathbf{n}).$$

- The jump of a function f across S_j is denoted by:

$$[f]_{S_j} = f_{S_j}^- - f_{S_j}^+,$$

- $\partial_{\mathbf{n}} V = \mathbf{n} \cdot \nabla V$ denotes the partial derivative of V in the direction of a unit vector \mathbf{n} ,
- The function $G(\mathbf{r}) = \frac{1}{4\pi\|\mathbf{r}\|}$ is the fundamental solution of the Laplacian in \mathbb{R}^3 , such that $-\Delta G = \delta_0$.

Consider an open region Ω and a function u such that $\Delta u = 0$ in Ω and in $\mathbb{R}^3 \setminus \Omega$ (but not necessarily continuous across $\partial\Omega$). The Green Representation Theorem states that, for a point \mathbf{r} belonging to $\partial\Omega$,

$$\frac{u^-(\mathbf{r}) + u^+(\mathbf{r})}{2} = - \int_{\partial\Omega} [u] \partial_{\mathbf{n}'} G(\mathbf{r} - \mathbf{r}') ds(\mathbf{r}') + \int_{\partial\Omega} [\partial_{\mathbf{n}'} u] G(\mathbf{r} - \mathbf{r}') ds(\mathbf{r}') . \quad (4)$$

This representation also holds for the head model in Figure 1, when Ω is the union of disjoint open sets: $\Omega = \Omega_1 \cup \Omega_2 \cup \dots \cup \Omega_N$, with $\partial\Omega = S_1 \cup S_2 \cup \dots \cup S_N$. If u is harmonic in each Ω_i , for $\mathbf{r} \in S_i$,

$$\frac{u^-(\mathbf{r}) + u^+(\mathbf{r})}{2} = - \sum_{j=1}^N \left(\int_{S_j} [u]_{S_j} \partial_{\mathbf{n}'} G(\mathbf{r} - \mathbf{r}') ds(\mathbf{r}') + \int_{S_j} [\partial_{\mathbf{n}'} u]_{S_j} G(\mathbf{r} - \mathbf{r}') ds(\mathbf{r}') \right) \quad (5)$$

The notation is simplified by introducing two integral operators, which map a scalar function f on $\partial\Omega$ to another scalar function on $\partial\Omega$: the “double-layer” operator $(\mathcal{D}f)(\mathbf{r}) = \int_{\partial\Omega} \partial_{\mathbf{n}'} G(\mathbf{r} - \mathbf{r}') f(\mathbf{r}') ds(\mathbf{r}')$, and the “single-layer” operators $(\mathcal{S}f)(\mathbf{r}) = \int_{\partial\Omega} G(\mathbf{r} - \mathbf{r}') f(\mathbf{r}') ds(\mathbf{r}')$. For an operator \mathcal{D} , its restriction \mathcal{D}_{ij} maps a function of S_j to a function of S_i .

An extension of the Green Representation Theorem represents the directional derivative of a harmonic function as a combination of boundary integrals of higher order. This requires two more integral operators: the adjoint \mathcal{D}^* of the double-layer operator, and a hyper-singular operator \mathcal{N} defined by

$$(\mathcal{N}f)(\mathbf{r}) = \int_{\partial\Omega} \partial_{\mathbf{n}, \mathbf{n}'} G(\mathbf{r} - \mathbf{r}') f(\mathbf{r}') ds(\mathbf{r}'). \text{ If } \mathbf{r} \text{ is a point of } S_i, \quad (6)$$

$$-\frac{\partial_{\mathbf{n}} u^-(\mathbf{r}) + \partial_{\mathbf{n}} u^+(\mathbf{r})}{2} = \mathcal{N}[u] - \mathcal{D}^*[\partial_{\mathbf{n}} u],$$

where \mathcal{D}^* is the adjoint of the operator \mathcal{D} . The Geselowitz formula exploits only the first boundary integral representation equation (5), while it is possible to exploit both (5) and (6). Thus three Boundary Element Methods can be derived within a unified setting: a BEM involving only single-layer potentials, a BEM involving only double-layer potentials, and a symmetric BEM combining single- and double-layer potentials [17]. We concentrate hereforth on the double-layer and on the symmetric BEMs.

The double-layer BEM

To apply the representation theorem to the forward problem of EEG, a harmonic function must be produced, which relates the potential and the sources. Decomposing the source term as $f = \sum_i f_i$ where the support of each f_i lies inside Ω_i , consider v_{Ω_i} such that $\Delta v_{\Omega_i} = f_i$ holds in all \mathbb{R}^3 . The function $v_d = \sum_{i=1}^N v_{\Omega_i}$ satisfies $\Delta v_d = f$ and is continuous across each surface S_i , as well as its normal derivative $\partial_{\mathbf{n}} v_d$. The function $u = \sigma V - v_d$ is a harmonic function in Ω , to which (5) can be applied. Since $[u]_{S_i} = (\sigma_i - \sigma_{i+1})V_{S_i}$ and $[\partial_{\mathbf{n}} u] = 0$, we obtain, on each surface S_i ,

$$\frac{\sigma_i + \sigma_{i+1}}{2} V_{S_i} + \sum_{j=1}^N (\sigma_j - \sigma_{j+1}) \mathcal{D}_{ij} V_{S_j} = v_d. \quad (7)$$

The above formula was established by Geselowitz [10], and was the only one used to model electroencephalography or electrocardiography, until recently, when [17] showed the diversity of BEMs that

can be derived. This classical BEM is called a double-layer BEM because it only involves the double-layer operator \mathcal{D} .

The symmetric BEM

The originality of the symmetric Boundary Element Method is to consider a different piecewise harmonic function for each domain: the function u_{Ω_i} equal to $V - \frac{v_{\Omega_i}}{\sigma_i}$ within Ω_i and to $-\frac{v_{\Omega_i}}{\sigma_i}$ outside of Ω_i . This u_{Ω_i} is indeed harmonic in $\mathbb{R}^3 \setminus \partial\Omega_i$, and the representation equations (5) and (6) can be applied, leading to a system of integral equations involving two types of unknowns: the potential V_i and the normal current $(\sigma\partial_{\mathbf{n}}V)_i$ on each interface.

The surfaces are represented by triangular meshes. To fix ideas, consider a three-layer geometrical model for the head. Conductivities of each domain are respectively denoted σ_1 , σ_2 and σ_3 . The surfaces enclosing these homogeneous conductivity regions are denoted S_1 (inner skull boundary), S_2 (skull-scalp interface) and S_3 (scalp-air interface). Denoting $\psi_i^{(k)}$ the P0 function associated to triangle i on surface S_k , and $\phi_j^{(l)}$ the P1 function associated to node j on surface S_l , the potential V on surface S_k is approximated as $V_{S_k}(\mathbf{r}) = \sum_i x_i^{(k)} \phi_i^{(k)}(\mathbf{r})$, while $p = \sigma\partial_{\mathbf{n}}V$ on surface S_k is approximated by $p_{S_k}(\mathbf{r}) = \sum_i y_i^{(k)} \psi_i^{(k)}(\mathbf{r})$. As an illustration, considering the source term to reside in the brain compartment Ω_1 , the variables $(\mathbf{x}_k)_i = x_i^{(k)}$ and $(\mathbf{y}_k)_i = y_i^{(k)}$ satisfy the linear system:

$$\begin{bmatrix} \hat{\sigma}_{12}\mathbf{N}_{11} & -2\mathbf{D}_{11}^* & -\sigma_2\mathbf{N}_{12} & \mathbf{D}_{12}^* & 0 \\ -2\mathbf{D}_{11} & \hat{\sigma}_{12}\mathbf{S}_{11} & \mathbf{D}_{12} & -\sigma_2^{-1}\mathbf{S}_{12} & 0 \\ -\sigma_2\mathbf{N}_{21} & \mathbf{D}_{21}^* & \hat{\sigma}_{23}\mathbf{N}_{22} & -2\mathbf{D}_{22}^* & -\sigma_3\mathbf{N}_{23} \\ \mathbf{D}_{21} & -\sigma_2^{-1}\mathbf{S}_{21} & -2\mathbf{D}_{22} & \hat{\sigma}_{23}\mathbf{S}_{22} & \mathbf{D}_{23} \\ 0 & 0 & -\sigma_3\mathbf{N}_{32} & \mathbf{D}_{32}^* & \sigma_3\mathbf{N}_{33} \end{bmatrix} \begin{bmatrix} \mathbf{x}_1 \\ \mathbf{y}_1 \\ \mathbf{x}_2 \\ \mathbf{y}_2 \\ \mathbf{x}_3 \end{bmatrix} = \begin{bmatrix} \mathbf{b}_1 \\ \mathbf{c}_1 \\ 0 \\ 0 \\ 0 \end{bmatrix}$$

where $\hat{\sigma}_{ij}$ (resp. $\check{\sigma}_{ij}$) is defined as $\sigma_i + \sigma_j$ (resp. $\sigma_i^{-1} + \sigma_j^{-1}$) and where \mathbf{b}_1 and \mathbf{c}_1 are the coefficients of the P0 (resp. P1) boundary element decomposition of the source term $\partial_{\mathbf{n}}v_{\Omega_1}$ (resp. $-\sigma_1^{-1}v_{\Omega_1}$).

Blocks \mathbf{N}_{ij} and \mathbf{D}_{ij} map a potential V_j on S_j to a function defined on S_i . Block \mathbf{S}_{ij} maps a normal current p_j on S_j to a function defined on S_i . The resulting matrix is block-diagonal, and symmetric, hence the name “symmetric BEM”.

The magnetic field is computed from the electric field and the primary source distribution using the Biot and Savart equation (3), as proposed by Ferguson, Zhang and Stroink [9].

In summary, the symmetric BEM introduces an additional unknown into the problem: the normal current, and uses an additional set of representation equations linking the normal current and the potential. The symmetric BEM departs from the double-layer BEM in several ways:

- the normal current to each surface is explicitly modeled;

- only the surfaces which bound a common compartment have an interaction (whence the blocks of zeros in the matrix);
- only the surfaces which bound a compartment containing sources have a source term;
- the matrix is symmetric;
- the matrix is larger for a given head model.

OpenMEEG: Hands-on tutorial

OpenMEEG file formats

OpenMEEG handles several file formats corresponding to several type of objects: vectors, matrices, head geometries, meshes, dipoles, conductivities.

Vectors and matrices

By default matrices and vectors are stored on disk using a MATLAB file format. Symmetric matrices which are not directly representable in the MATLAB format are represented as a MATLAB struct. Other vector/matrices file formats are also supported. Forcing a specific file format is achieved by specifying the proper file extension. Matlab extension is `.mat`. Other useful file formats are ASCII (extension `.txt`) which generates human readable files, BrainVisa⁷ texture file format (extension `.tex`) and OpenMEEG's own binary file format (extension `.bin`) which is available solely for backward compatibility and should be considered as deprecated (as it is subsumed by the MATLAB file format).

Geometrical model, mesh and conductivity files

OpenMEEG geometrical models are provided through several files. Note that OpenMEEG considers SI units (i.e. point coordinates should be expressed in meters (m), conductivities in S/m , etc). The toplevel file (generally ending with the extension `.geom`) assembles various interface descriptions to build *Domains* corresponding to head tissues. Empty lines or lines beginning with `#` are non-significant. The file must start with a special comment line which allows its identification (see example in Figure 9).

Geometrical models globally contain 2 sections.

The first section specifies the meshes of the interfaces between tissues. It is introduced by the keyword **Interfaces** followed by the number of such meshes followed by the keyword **Mesh** (which gives the type of the mesh description, **Mesh** being currently the only possibility). This specification is then followed by the

⁷<http://www.brainvisa.info>

names of – mesh – files describing each of the interfaces. Each interface is assigned an index from its order in the list. These indices start at 1.

The second section describes the head tissues and is introduced by the keyword **Domains** followed by the number of such domains. Each domain is then depicted, one domain per line, by the keyword **Domain** followed by the domain name (which will serve for identification and will also appear in the conductivity description) followed by a list of integers. These integer are the indices of the mesh files (as depicted in previous paragraph). They are affected by a + or - sign depending on whether the domain is outside or inside the corresponding interface (as defined by the outward normal of the interface). See Figure 9 for a detailed example.

Mesh files (generally ending with the **.tri** extension) follow the BrainVisa⁸ file format for meshes. These files contain two sections. Each section is introduced by the character - appearing at the beginning of the line followed by a space followed by either one number (first section) or three times the same number (second section).

The first section contains a list of points with associated normals. The number on the line introducing the section is the number of points. Each following line corresponds to a single point. Its coordinates are the three first numbers appearing on the line. The normal corresponds to the following three numbers. Each point is assigned an index (starting at 0) corresponding to its order of appearance in the list.

The second section contains the triangles of the mesh. The number (repeated three times) in the section delimiter corresponds to the number of triangles. Each triangle is depicted by a sequence of three integers corresponding to the indices of the points assigned as explained in the previous paragraph.

The following small example describes a very simple mesh containing 4 points and 4 triangles.

```
- 4
0 0 0 -0.5773 -0.5773 -0.5773
1 0 0 1 0 0
0 1 0 0 1 0
0 0 1 0 0 1
- 4 4 4
0 1 2
0 1 3
0 2 3
1 2 3
```

The interface meshes are required to be closed in order for the Boundary Element Method to function correctly. This is also necessary for the source meshes when computing forward solutions using surfacic

⁸Please note that FreeSurfer also provides **.tri** files. Those are not handled by OpenMEEG yet.

source models (see below). Moreover, the interface meshes must not intersect each other. Non-intersection can be checked with the command `om_check_geom`. The command `om_mesh_info` applied to a mesh provides its number of points, of triangles, minimum and maximum triangle area, and also its Euler characteristic. The Euler characteristic of a closed mesh of genus 0 (homotopic to a sphere) is equal to 2. The Euler characteristic gives an indication if a mesh is likely to be closed or not.

A **conductivity file** (generally ending with the extension `.cond`) is a simple ASCII file that contains associations between tissue names and conductivity values. Associations are provided one per line. Empty lines or lines beginning with `#` are non-significant. The file must start with a special comment line which allows its identification. Figure 10 provides an example conductivity file corresponding to the geometry file of figure 9.

Note that the tissue names are the ones appearing in the *Domain description* section of the file depicting the geometrical model.

Source description

Sources may be represented either by a surfacic distribution of dipoles, or by isolated dipoles.

A **surfacic distribution** can be defined by a mesh that supports the dipoles. The dipole orientations are then constrained to the normal direction to the mesh and the moment amplitude is modelled as continuous across the mesh (piecewise linear). Source values are defined at the mesh vertices.

Isolated dipoles are defined by a simple ASCII file as shown in Figure 11.

Sensor description

EEG sensors are supposed pointlike and are represented by their names and positions (x,y,z coordinates).

MEG sensors are represented by their names, positions, orientations and weighting coefficients.

Gradiometers can hence be defined by the linear combination of two magnetometers with opposite weights.

These parameters are defined by an ASCII file as shown in Figure 12.

OpenMEEG from the command line

This section reviews the main OpenMEEG command line tools. The general syntax and main options of each command is briefly provided. Full details are available in OpenMEEG documentation and figure 13 on page 36 provides a flowchart summarizing the use of these commands. *In this section, command names are in red, options are in green and produced files are shown in blue.*

om_assemble General syntax:

`om_assemble` Option Parameters Matrix

This program assembles the different matrices that will be used in later stages. It uses the head description, the sources and the sensors information. `Option` selects the type of matrice to assemble. `Parameters` depends on the specific option `Option`. Except if otherwise noted, it takes the form:

`subject.geom subject.cond OptParam`

where `subject.geom` and `subject.cond` are files describing respectively the geometrical model and the conductivities of the head (see above for a short description of these files). `OptParam` depends on the actual `Option`. `Matrix` is the name of the output file containing the computed matrix.

We now detail the possible `Options` (with their abbreviated versions given in parentheses), allowing to define various matrices to assemble:

General options for `om_assemble`

`-help` (`-h`, `--help`): summarizes all possible options.

Head modelling options for `om_assemble` produce matrices linked to the propagation of electrical signals in the head.

`-HeadMat` (`-HM`, `-hm`): `om_assemble` computes the Head matrix for Symmetric BEM (left-hand side of the linear system presented in the first appendix). This matrix corresponds to the propagation of electrical signals within the head. There is no `OptParam` in this case.

Source modelling options for `om_assemble` compute the source matrix for Symmetric BEM (right-hand side of the linear system). This matrix maps the representation of \mathbf{J}^P to its associated electric potential in an infinite medium (v_{Ω_1} in previous Appendix). Different options exist for the 2 types of source models:

`-SurfSourceMat` (`-SSM`, `-ssm`): should be used for continuous surfacic distributions of dipoles. `OptParam` is a file containing a mesh that describes the surface.

`-DipSourceMat` (`-DSM`, `-dsm`): should be used when considering several isolated dipoles. This model is the most commonly used and should be used by default even if the dipoles correspond to the vertices of a cortical mesh. `OptParam` is a file containing the dipolar source description.

Sensor modelling options for `om_assemble` compute matrices that integrate source information and computed potentials to provide the actual solution of the forward problem. The situation is slightly different for EEG, which only needs to compute the electric potential, and for MEG, which depends both on the electric potential and on the sources:

`-Head2EEGMat (-H2EM, -h2em)`: `om_assemble` computes the interpolation matrix that maps potentials computed on the scalp to EEG sensors. `OptParam` is a file describing the EEG sensor positions.

`-Head2MEGMat (-H2MM, -h2mm)`: `om_assemble` computes the contribution of Ohmic currents to the MEG sensors. `OptParam` is a file describing the SQUIDS geometries and characteristics.

`-Head2InternalPotMat (-H2IPM, -h2ipm)`: `om_assemble` computes the matrix that allows the computation of potentials at internal positions from potentials and normal currents on head interfaces, as computed by the symmetric BEM.

`-SurfSource2MEGMat (-SS2MM, -ss2mm)`: `om_assemble` computes the source contribution to the MEG sensors using the same source model as the one used for the option `-SurfSourceMat`, i.e. surfacic distribution of dipoles. For this option, `OptParam` takes the form:

`mesh squids`

where `mesh` contains a mesh describing the source surface and `squids` is a file describing the SQUIDS geometries and characteristics.

`-DipSource2MEGMat (-DS2MM, -ds2mm)`: `om_assemble` computes the source contribution to the MEG sensors using the same source model as the one used for the option `-DipSourceMat`, i.e. isolated dipoles. For this option, `OptParam` takes the form:

`dipoles squids`

where `dipoles` contains the dipolar source description and `squids` is a file describing the SQUIDS geometries and characteristics.

`-DipSource2InternalPotMat (-DS2IPM, -ds2ipm)`: `om_assemble` computes the source contribution to the chosen internal points. It gives the potential due to isolated dipoles, as if the medium were infinite. For this option, `OptParam` takes the form:

`dipoles internalPoints`

where `dipoles` contains the dipolar source description and `internalPoints` is a file describing the points locations.

EIT options for `om_assemble`

`-EITSourceMat (-EITSM, -EITsm,)`: `om_assemble` computes the right-hand side for scalp current injection. This usage of `om_assemble` outputs the right-hand side vector for a given set of EIT electrode. For this option, `OptParam` is a file describing the EIT electrode positions.

om_minverser General syntax:

```
om_minverser HeadMat HeadMatInv
```

This program is used to invert the symmetric matrix as provided by the command **om_assemble** with the option **-HeadMat**. This command has only one option.

-help (**-h**,**--help**): summarizes the usage of **om_minverser**.

om_gain General syntax:

```
om_gain Option HeadMatInv Parameters GainMatrix
```

This command computes the gain matrix by multiplying together matrices obtained previously (e.g. **HeadMatInv** is the matrix computed using **om_minverser**). The resulting gain matrix is stored in the file **GainMatrix**. **Option** selects the type of matrice to build. **Parameters** depend on the specific option **Option**. Possible options are:

General options

-help (**-h**,**--help**): summarizes the usage of **om_gain** for all its possible options.

Gain matrix type options select the type of gain matrix to be computed by **om_gain**.

-EEG : allows to compute an EEG gain matrix.

Parameters are then:

```
HeadMatInv SourceMat Head2EEGMat
```

SourceMat is the matrix obtained using **om_assemble** with either of the options **-SurfSourceMat** or **-DipSourceMat**, depending on the source model. **Head2EEGMat** is the matrix obtained using **om_assemble** with the option **-Head2EEGMat**.

The **-EEG** option can also be used to compute an EIT gain matrix (see below for the signification of the parameters in this case).

-EIT : allows to compute an EIT gain matrix. This option is actually an alias for the **-EEG** option in newer versions. For OpenMEEG versions 2.0 and below please use the **-EEG** option. **Parameters** are thus:

```
HeadMatInv SourceMat Head2EITMat
```

SourceMat should contain the output of the **-EITsource** option of **om_assemble**. Multiplying the EIT gain matrix by the vector of applied currents at each EIT electrode yields the simulated

potential on the EEG electrodes. The applied current on the EIT electrodes should sum to zero.

The result is stored in the file `Head2EITMat`

`-MEG` : allows to compute an MEG gain matrix.

Parameters are then:

`HeadMatInv SourceMat Head2MEGMat Source2MEGMat`

`SourceMat` is the matrix obtained using `om_assemble` with either of the options `-SurfSourceMat` or `-DipSourceMat`, depending on the source model. `Head2MEGMat` is the matrix obtained using `om_assemble` with the option `-HeadMEEGMat`. `Source2MEGMat` is the matrix obtained using `om_assemble` with either of the options `-SurfSource2MEGMat` or `-DipSource2MEGMat`, depending on the source model.

`-InternalPotential` : allows to compute an internal potential gain matrix for sensors within the volume.

Parameters are then:

`HeadMatInv SourceMat Head2InternalPotMat Source2InternalPotMat`

`Head2InternalPotMat` and `Source2InternalPotMat` are respectively obtained using `om_assemble` with option `-Head2InternalPotMat` and `-DipSource2InternalPotMat`.

Examples

Assuming a head model represented by the geometry file `head.geom` and the conductivity file `head.cond` and EEG sensors detailed in a file `head.eegsensors`. Computing the EEG gain matrix for sources distributed on the surface represented by the file `sources.tri` is done via the following set of commands:

```
om_assemble -HeadMat head.geom head.cond head.hm
om_assemble -SSM head.geom head.cond sources.tri head.ssm
om_assemble -h2em head.geom head.cond head.eegsensors head.h2em
om_minverser head.hm head.hm_inv
om_gain -EEG head.hm_inv head.ssm head.h2em head.gain
```

Considering now isolated dipolar sources detailed in the file `sources.dip` with MEG sensors depicted in the file `head.squids`. Using the same head model, the MEG gain matrix is obtained via the following set of commands:

```
om_assemble -HeadMat head.geom head.cond head.hm
om_assemble -DSM head.geom head.cond sources.dip head.dsm
om_assemble -h2mm head.geom head.cond head.squids head.h2mm
om_assemble -ds2mm sources.dip head.squids head.ds2mm
om_minverser head.hm head.hm_inv
om_gain -MEG head.hm_inv head.dsm head.h2mm head.ds2mm head.gain
```

Figures

Figure 1 - Models for Boundary Elements Methods

Boundary Elements are well-suited for piecewise constant isotropic conductivity models. OpenMEEG handles nested regions (left), and could in principle be extended to more general, disjoint regions (right) as presented in [18].

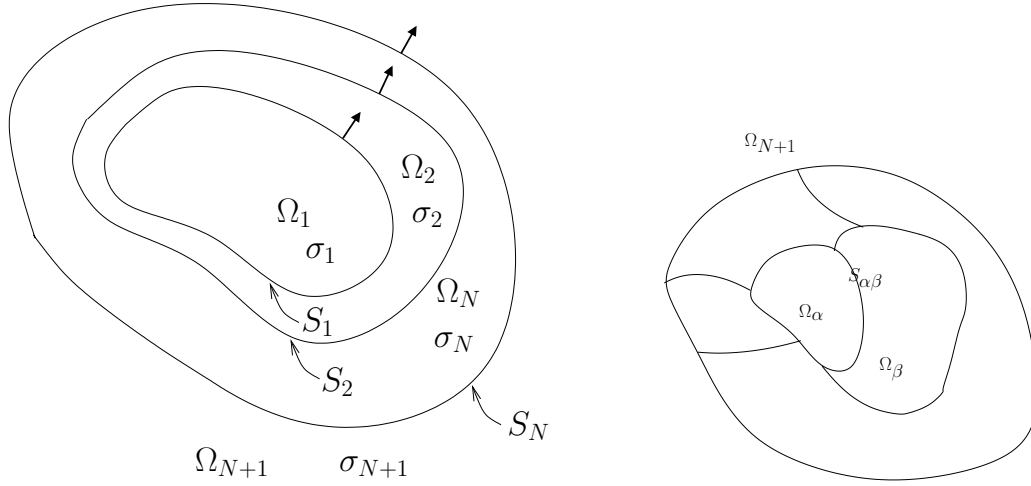


Figure 1:

Figure 2 - Head model made of 3 nested regular sphere meshes and 5 dipoles

Head model made of 3 nested regular sphere meshes with 5 dipoles close to the inner layer.

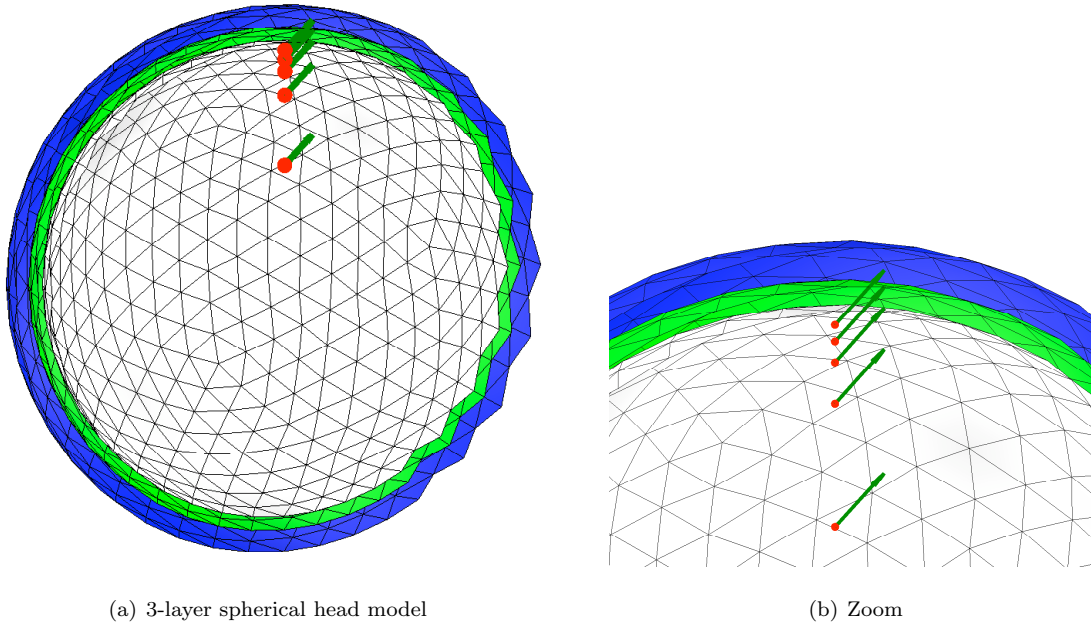


Figure 2:

Figure 3 - Accuracy comparison of the different BEM solvers for EEG

Forward EEG: accuracy comparison of different BEM solvers with three-layers sphere head models. We observe that the Symmetric BEM outperforms the other methods in term of precision.

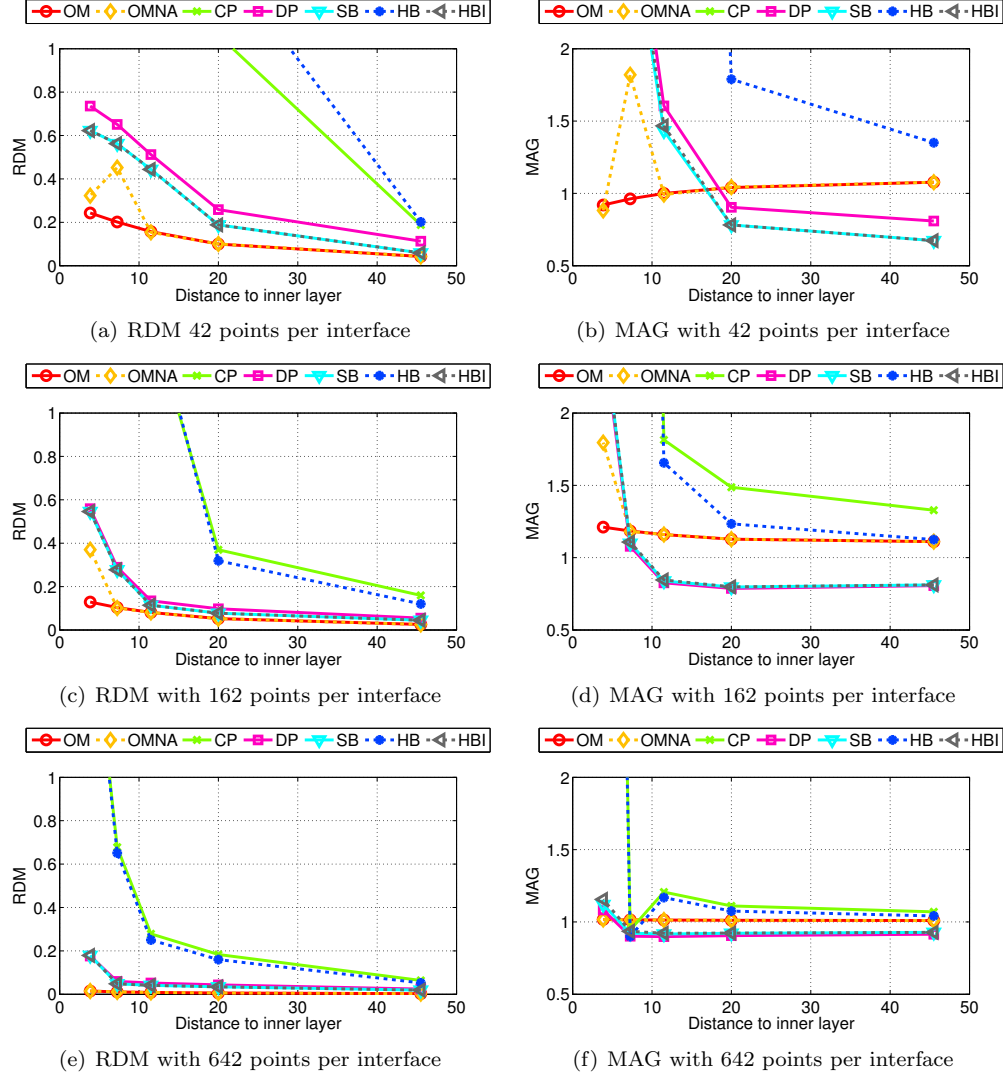


Figure 3:

Figure 4 - Accuracy comparison for EEG using random meshes with fixed number of vertices

Forward EEG: RDM and MAG boxplots obtained on 100 random 3-layers sphere models. Each layer contains 600 or 800 random vertices.

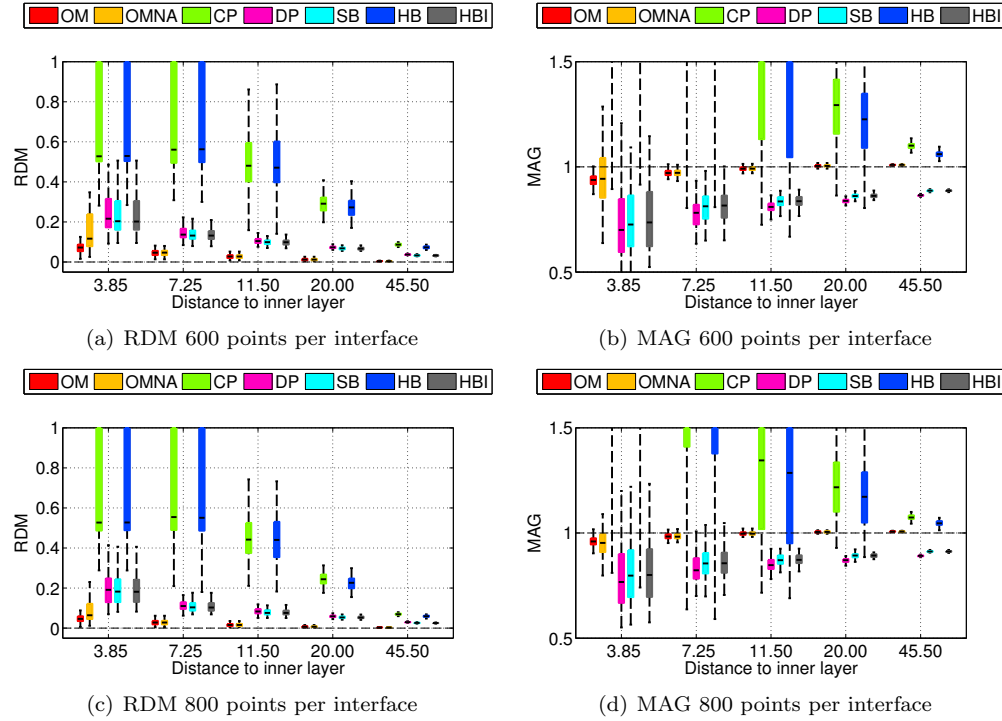


Figure 4:

Figure 5 - Accuracy comparison for EEG using random meshes and fixed number of unknowns

Forward EEG: RDM and MAG boxplots obtained on 100 random 3-layers sphere models. Each forward solution is obtained taking as constraint that the number of unknowns that is estimated is the same for all BEM solvers. Results are presented for 1500 and 3000 unknowns.

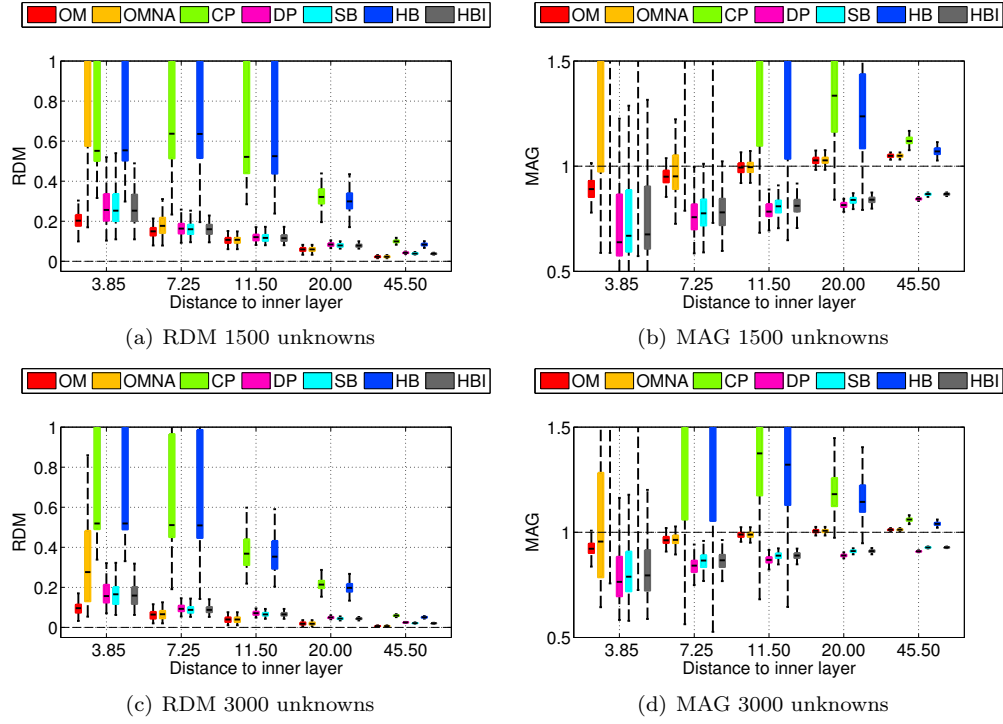


Figure 5:

Figure 6 - Accuracy comparison for MEG using random meshes with fixed number of vertices and non-radial magnetometers

Forward MEG: RDM and MAG boxplots obtained on 100 random sphere models (1 and 3-layers) using **non-radial magnetometers**. Each layer contains 600 or 800 random vertices.

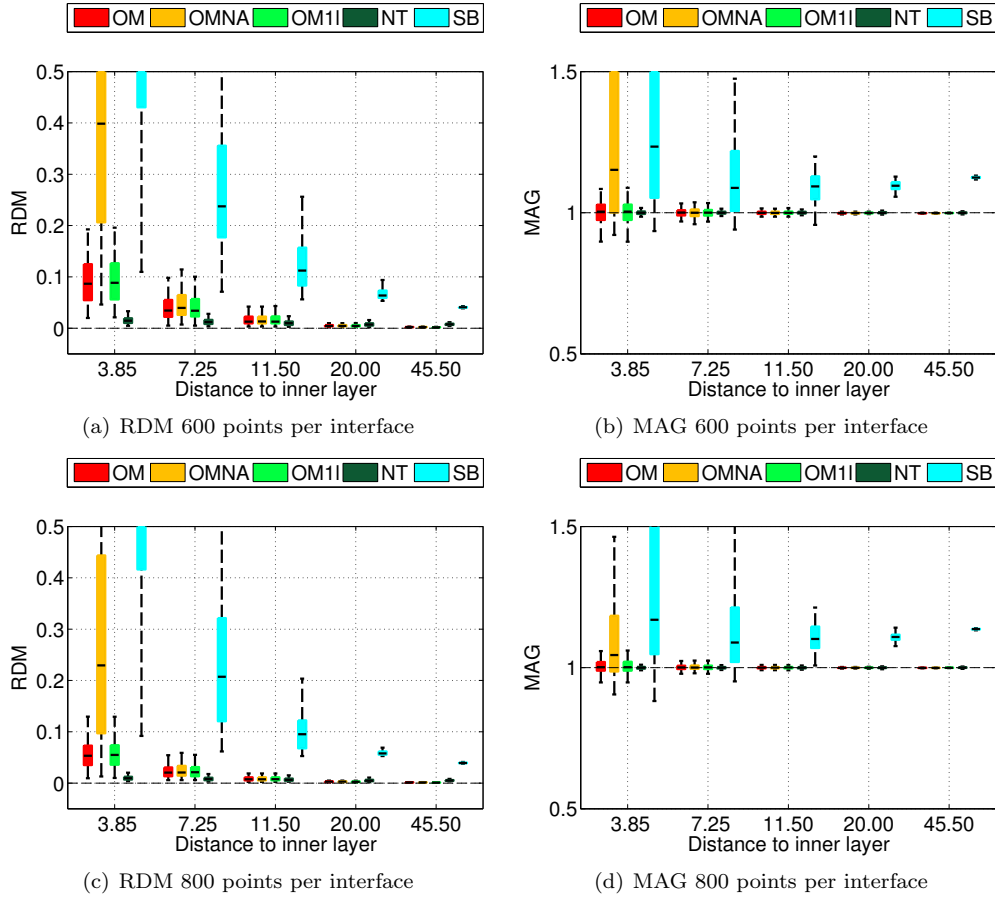


Figure 6:

Figure 7 - Accuracy comparison for MEG using random meshes with fixed number of vertices and radial magnetometers

Forward MEG: RDM and MAG boxplots obtained on 100 random sphere models (1 and 3-layers) using radial magnetometers. Each layer contains 600 or 800 random vertices.

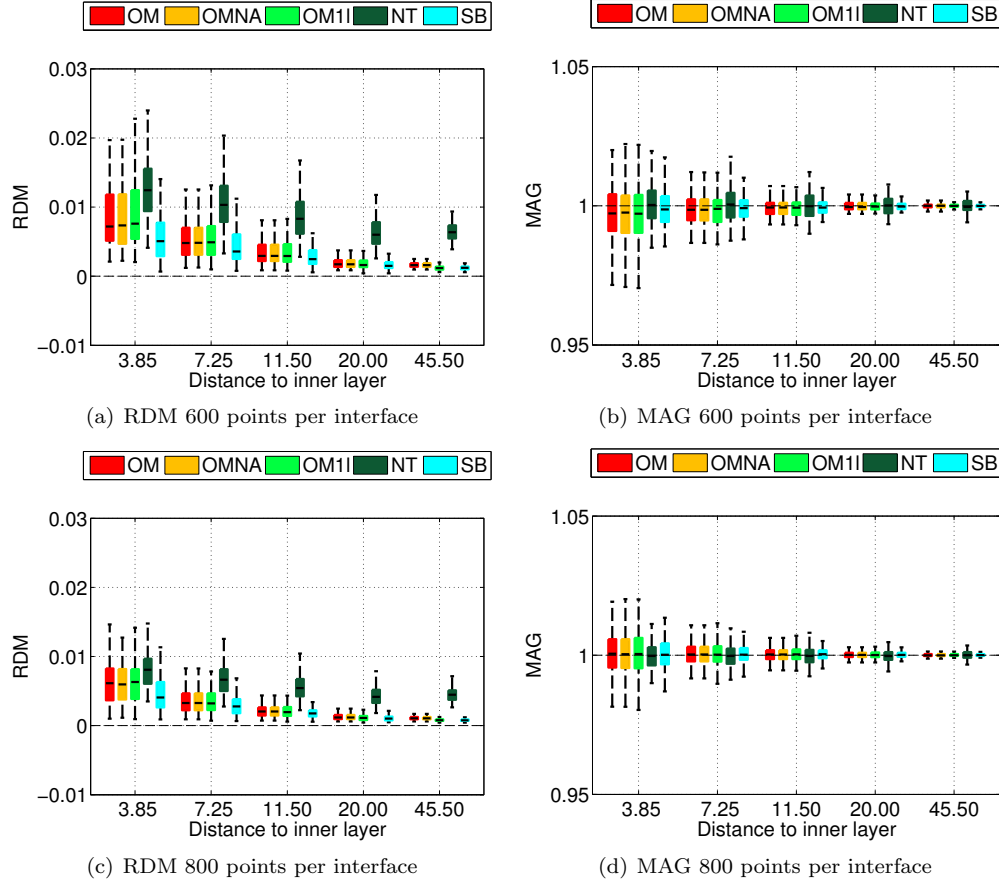


Figure 7:

Figure 8 - Computation times of the different BEM solvers for EEG

Forward EEG: computation times for the different solvers as a function of the number of vertices per layer or the number of unknowns.

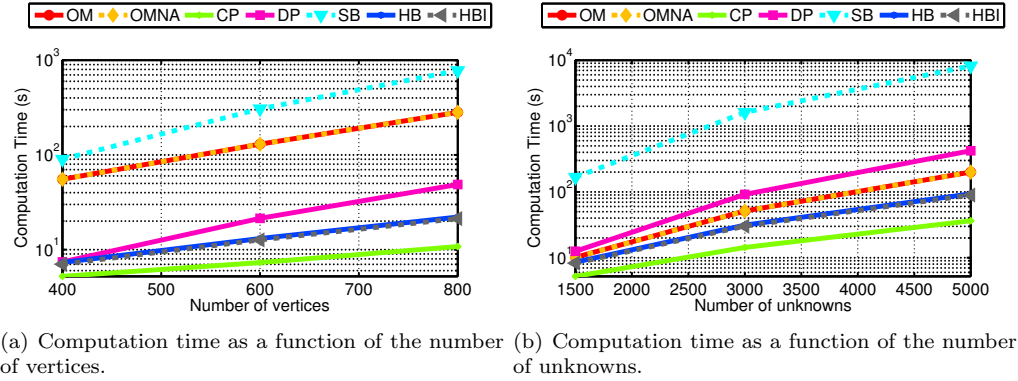


Figure 8:

Figure 9 - Sample geometry file

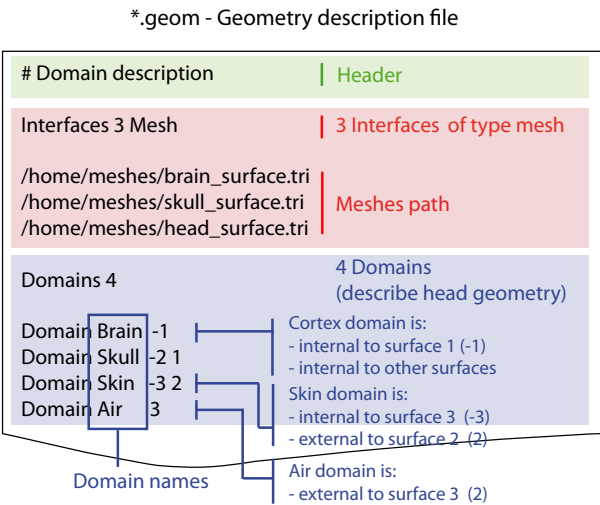


Figure 9:

Figure 10 - Sample conductivity file

Sample conductivity file and its correspondence with the geometry file.

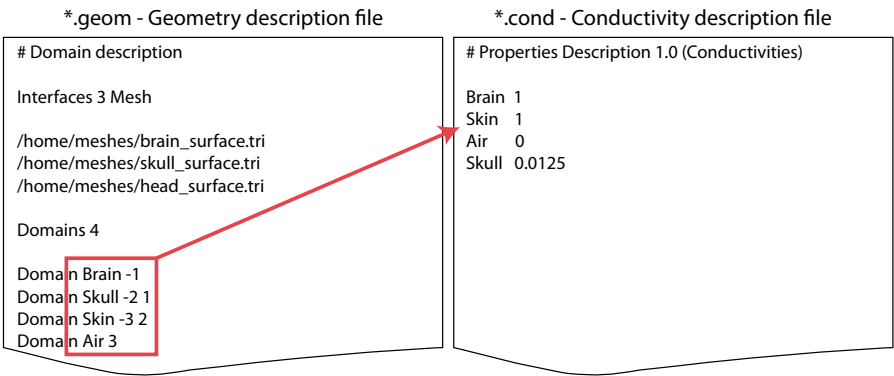


Figure 10:

Figure 11 - Sample source description for isolated dipoles.

Dipoles positions and orientations description file

| | | | | | | |
|---|---|--------|--------|---|--------|------------------------------------|
| 0 | 0 | 0.4250 | 0.7071 | 0 | 0.7071 | |
| 0 | 0 | 0.6800 | 0.7071 | 0 | 0.7071 | |
| 0 | 0 | 0.7650 | 0.7071 | 0 | 0.7071 | Dipole 3: |
| 0 | 0 | 0.8075 | 0.7071 | 0 | 0.7071 | - position : (0, 0, 0.7650) |
| 0 | 0 | 0.8415 | 0.7071 | 0 | 0.7071 | - orientation: (0.7071, 0, 0.7071) |

Positions: Cartesian coordinates Orientations: Cartesian coordinates
of moment direction

Figure 11:

Figure 12 - Sample sensors description for EEG and MEG.

*.patches - Electrodes description file

| | | | |
|-------|---------|---------|---------|
| EEG00 | -0.5257 | 0.0000 | 0.8506 |
| EEG01 | 0.5257 | 0.0000 | 0.8506 |
| EEG02 | -0.5257 | 0.0000 | -0.8506 |
| EEG03 | 0.5257 | 0.0000 | -0.8506 |
| EEG04 | 0.0000 | 0.8506 | 0.5257 |
| EEG05 | 0.0000 | 0.8506 | -0.5257 |
| EEG06 | 0.0000 | -0.8506 | 0.5257 |
| EEG07 | 0.0000 | -0.8506 | -0.5257 |
| EEG08 | 0.8506 | 0.5257 | 0.0000 |
| EEG09 | -0.8506 | 0.5257 | 0.0000 |
| EEG10 | 0.8506 | -0.5257 | 0.0000 |
| EEG11 | -0.8506 | -0.5257 | 0.0000 |

labels electrodes positions (x,y,z)
(optional)

*.squids - MEG sensors description file

| | | | | | | | |
|-----|---------|---------|---------|---------|---------|---------|------|
| M00 | -0.6308 | 0.0000 | 1.0207 | -0.5257 | 0.0000 | 0.8506 | 1.0 |
| M01 | 0.6308 | 0.0000 | 1.0207 | 0.5257 | 0.0000 | 0.8506 | 1.0 |
| M02 | -0.6308 | 0.0000 | -1.0207 | -0.5257 | 0.0000 | -0.8506 | 1.0 |
| M03 | 0.6308 | 0.0000 | -1.0207 | 0.5257 | 0.0000 | -0.8506 | 1.0 |
| M04 | 0.0000 | 1.0207 | 0.6308 | 0.0000 | 0.8506 | 0.5257 | 1.0 |
| M05 | 0.0000 | 1.0207 | -0.6308 | 0.0000 | 0.8506 | -0.5257 | 1.0 |
| M06 | 0.0000 | -1.0207 | 0.6308 | 0.0000 | -0.8506 | 0.5257 | 1.0 |
| M07 | 0.0000 | -1.0207 | -0.6308 | 0.0000 | -0.8506 | -0.5257 | 1.0 |
| M08 | 1.0207 | 0.6308 | 0.0000 | 0.8506 | 0.5257 | 0.0000 | 1.0 |
| M09 | -1.0207 | 0.6308 | 0.0000 | -0.8506 | 0.5257 | 0.0000 | 1.0 |
| G10 | -1.0207 | -0.6308 | 0.0000 | 0.8506 | -0.5257 | 0.0000 | 1.0 |
| G10 | -1.0207 | -0.6212 | 0.1095 | -0.8506 | 0.5257 | 0.0000 | -1.0 |

labels squids positions squids orientations weights
(optional)

planar gradiometer description

Figure 12:

Figure 13 - Pipelines for computing leadfields with OpenMEEG.

Diagram for the low level pipeline for computing MEG and EEG leadfields (a.k.a., gain matrices) using OpenMEEG. To facilitate the understanding of this diagram one can give an example: An EEG gain matrix is obtained with the *om_gain* command using with option *-EEG* taking as input an inverted head matrix, an EEG sensors matrix and a source matrix. The source matrix can be obtained using *om_assemble* taking as input a head model (geometry and conductivities) and a source description file (option *-dsm* when using isolated dipoles). The inverted head matrix is obtained using *om_minverser* from a head matrix which is obtained using *om_assemble* and the option *-HM* from a head model (geometry and conductivities).

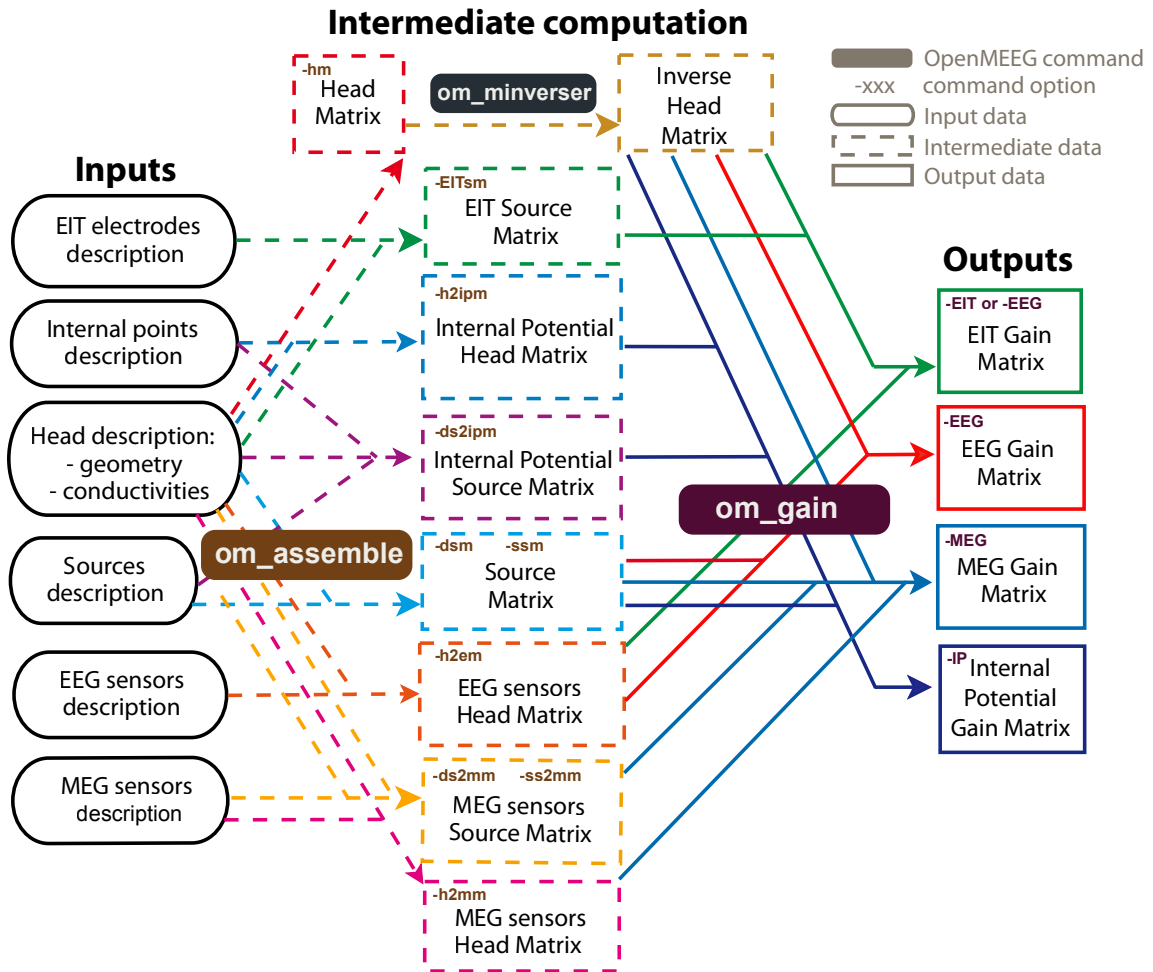


Figure 13:

Tables

Table 1 - OpenMEEG demo script in Python

Demo script for computing MEG and EEG forward problems with OpenMEEG in Python.

```
#!/usr/bin/env python
import openmeeeg as om

# Load data
condFile='om_demo.cond'
geomFile='om_demo.geom'
dipoleFile='cortex.dip'
squidsFile='meg_squids.txt'
electrodesFile='eeg_electrodes.txt'

geom = om.Geometry()
geom.read(geomFile,condFile)

dipoles = om.Matrix()
dipoles.load(dipoleFile)

squids = om.Sensors()
squids.load(squidsFile)

electrodes = om.Matrix()
electrodes.load(electrodesFile)

# Compute forward problem (Build Gain Matrices)
gaussOrder = 3; # Numerical integration order

hm      = om.HeadMat(geom,gaussOrder)
hminv   = hm.inverse()
dsm     = om.DipSourceMat(geom,dipoles,gaussOrder)
ds2mm   = om.DipSource2MEGMat(dipoles,squids)
h2mm    = om.Head2MEGMat(geom,squids)
h2em    = om.Head2EEGMat(geom,electrodes)
gain_meg = om.GainMEG(hminv,dsm,h2mm,ds2mm)
gain_eeg = om.GainEEG(hminv,dsm,h2em)
```

Table 1:

Table 2 - OpenMEEG demo script in Matlab

Demo script for computing an EEG forward problem with OpenMEEG in Fieldtrip.

```
%% The structure for the BEM volume conduction model
%% Each layer mesh is indexed by k
% vol.bnd(k).pnt : contains vertices for mesh "k"
% vol.bnd(k).tri : contains triangles for mesh "k"
%% Set the conductivities of each domain
% vol.cond       : contains conductivities

%% EEG electrodes
% sens.pnt       : contains locations of electrodes

%% Positions of the dipoles
% pos            : contains locations of dipoles

%% Compute the BEM
% choose BEM method (OpenMEEG, BEMCP or Dipoli)
cfg.method = 'openmeeg';
% Compute the BEM matrix
vol = ft_prepare_bemmodel(cfg, vol);
cfg.vol = vol;
cfg.grid.pos = pos;
cfg.elec = sens;
% Compute leadfield (no orientation constraint)
lf_openmeeg = ft_prepare_leadfield(cfg);
```

Table 2: